Adell et al., http://www.jcb.org/cgi/content/full/jcb.201310114/DC1



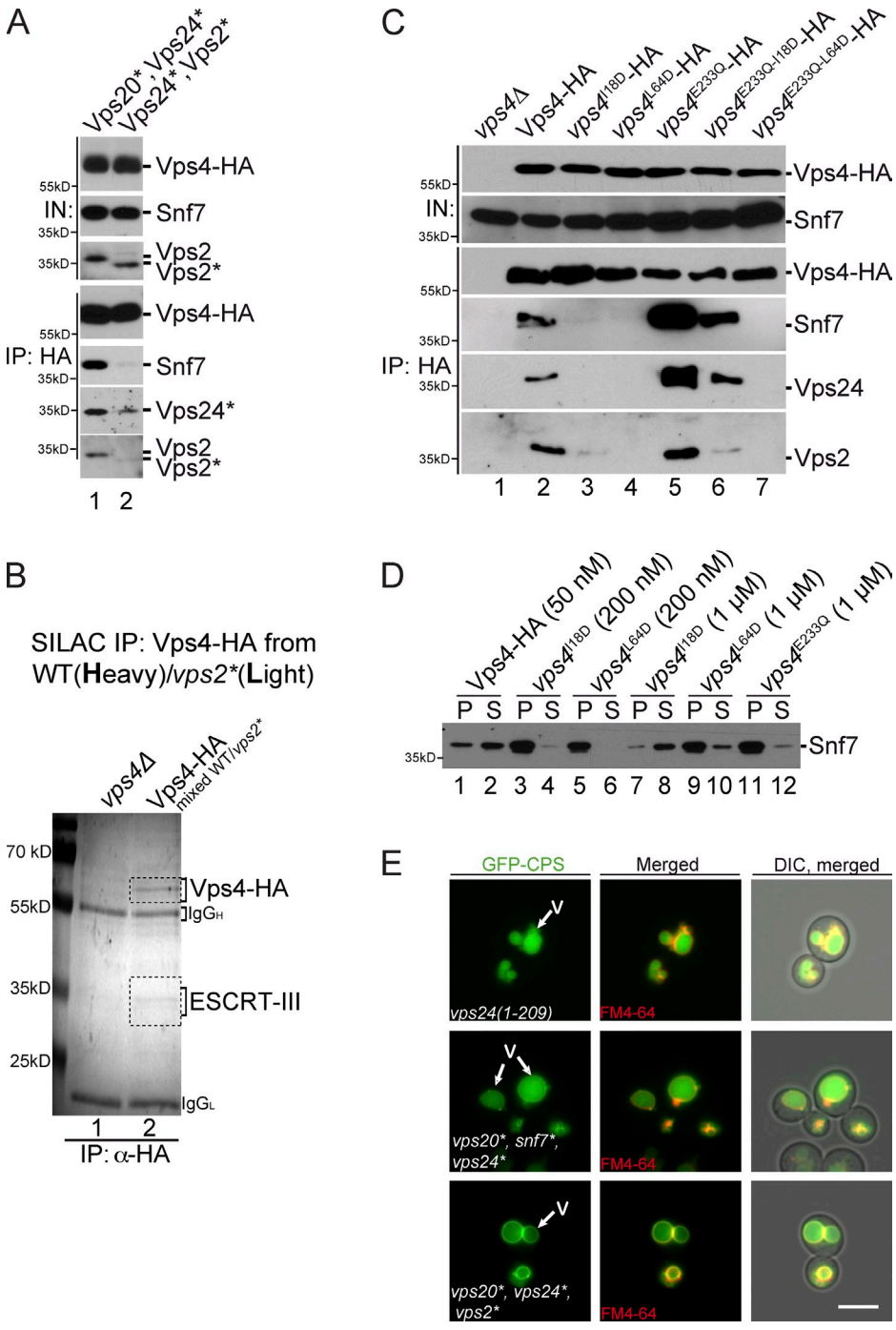


Figure S1. **Analysis of MIT–MIM interaction.** (A) Immunoprecipitation of Vps4-HA from cell lysates of *vps20*, vps24** and *vps24*, vps2** double mutants. (A and C) Immunoprecipitates were separated by SDS-PAGE and analyzed by Western blotting using the indicated antibodies. (B) Vps4-HA immunoprecipitates from WT cell lysates (labeled with [$^{13}C_6$/$^{15}N_2$] L-lysine) and from *vps2** cell lysates were mixed and subjected to SDS-PAGE and Coomassie staining. The indicated bands (dotted boxes) were excised, digested with LysC, and analyzed by mass spectrometry. (C) Immunoprecipitation (IP) of Vps4-HA, Vps4-E233Q-HA, and the respective MIT mutants from cell lysates. (D) Semi–in vitro disassembly assay with membrane fractions isolated from *vps4Δ* mutants. Membrane fractions were incubated with ATP and the indicated concentrations of recombinant Vps4, Vps4-I18D, or Vps5-L64D for 5 min. Membrane-associated proteins (13,000 *g* pellet [P]) and released proteins (13,000 *g* supernatant [S]) were separated by centrifugation and analyzed by SDS-PAGE and Western blotting. (E) Live-cell fluorescence microscopy of the indicated strains expressing GFP-CPS. DIC, differential interference contrast; IN, input; V, vacuole. Bar, 5 μM.

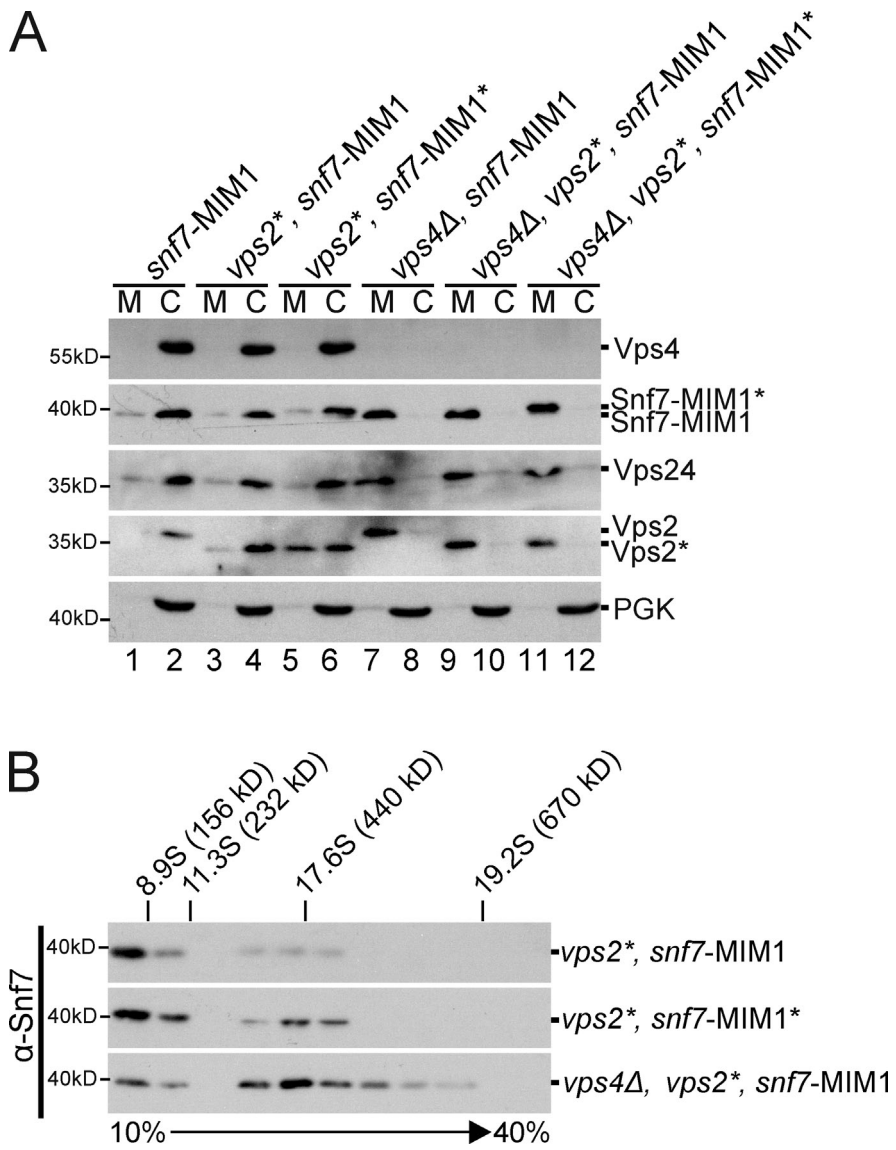


Figure S2. **Characterization of chimeric ESCRT-III complexes.** (A) Membrane fractions (M) and cytoplasmic fractions (C) of WT cells and the indicated mutants were analyzed by SDS-PAGE and Western blotting. (B) Solubilized membrane fractions (13,000 *g* pellet) of WT cells and the indicated MIM mutants were subjected to velocity sedimentation and analyzed by SDS-PAGE and Western blotting.

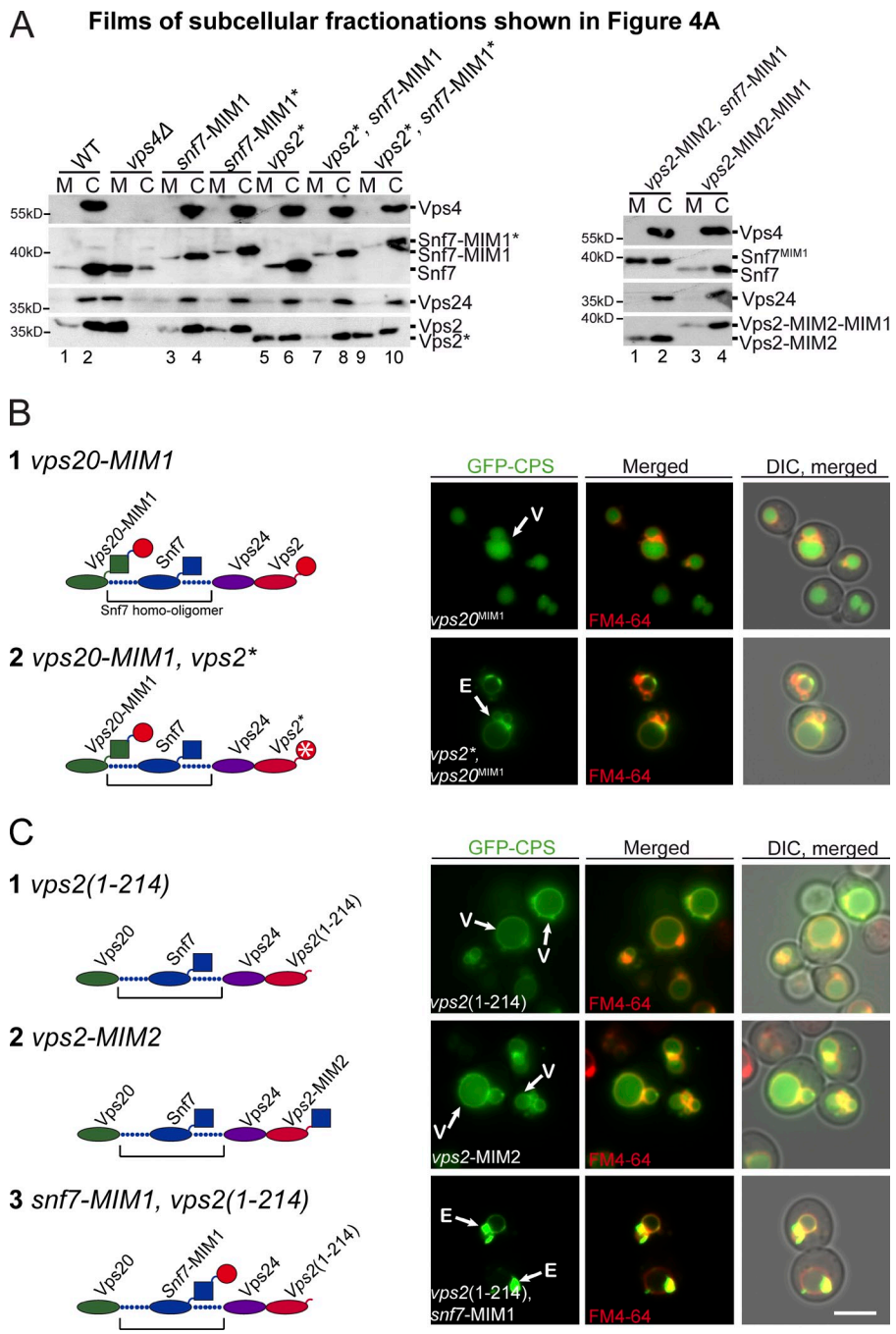


Figure S3. **Characterization of a *Vps20*$^{MIM1}$ chimera in MVB cargo sorting.** (A) Uncut Western blot films from the subcellular fraction analysis shown in Fig. 4 A sections 1–7. M, membrane fraction; C, cytoplasmic fraction. (B and C) Schematic representation of ESCRT-III complexes constructed with the indicated chimeras and the live-cell imaging of GFP-CPS of the corresponding strains. DIC, differential interference contrast; V, vacuole; E, class E compartment. Bar, 5 µM.

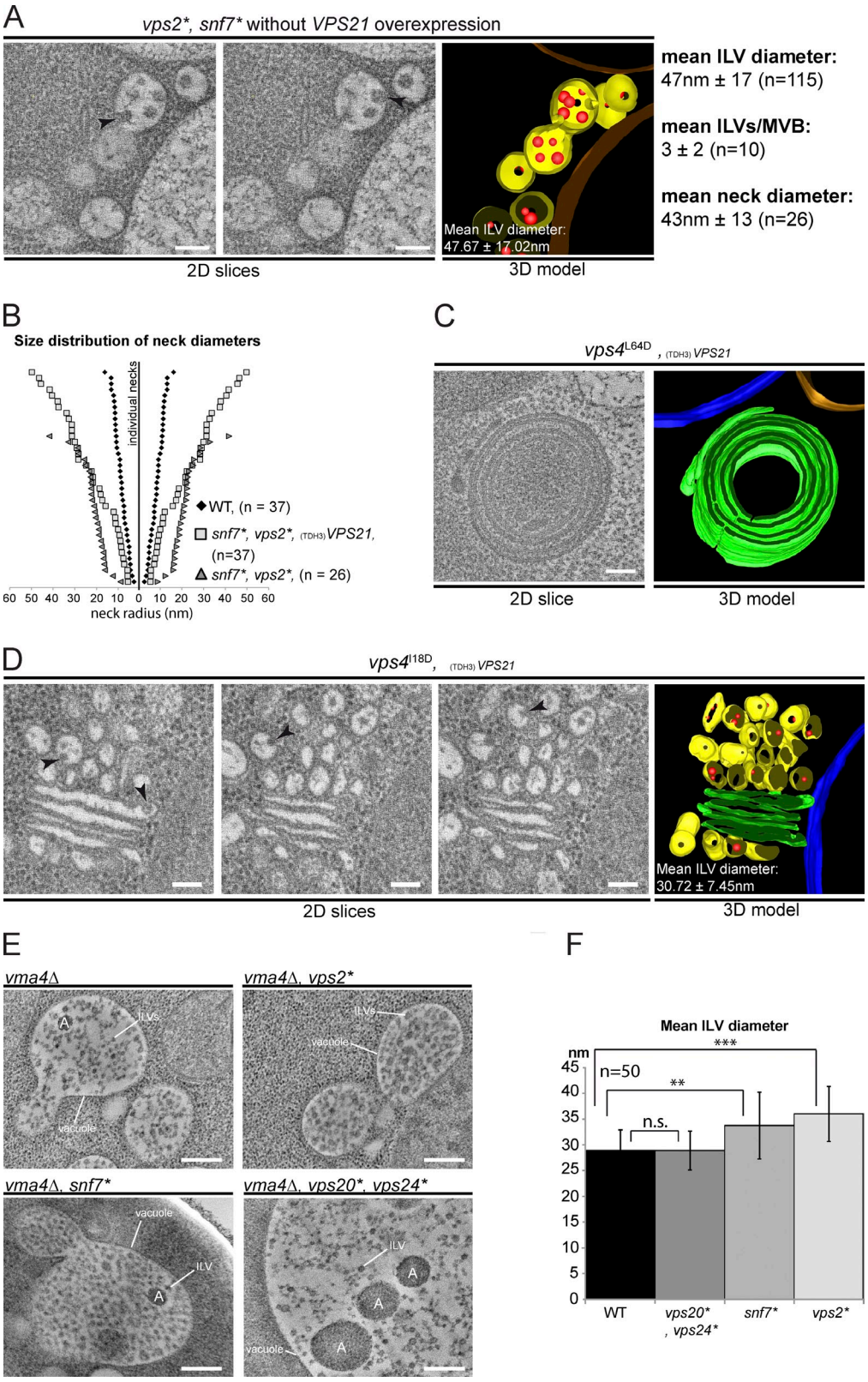


Figure S4. **Characterization of the MVB vesicle morphology.** (A) Electron tomography of cryofixed *snf7*, vps2** double mutants without *VPS21* overexpression. 2D slices from tomographic reconstructions and models from 400-nm sections are shown. Arrowheads point to enlarged budding profiles. Limiting MVB membrane (yellow), ILVs (red), and vacuole (brown). Bar, 150 nm. (B) Size distribution of individual membrane neck diameters of the WT and the indicated mutants. (C and D) Electron tomography of cryofixed Vps4-L64D (C) and Vps4-I18D (D) mutants. 2D slices from tomographic reconstructions and models from 400-nm sections are shown. Arrowheads point to enlarged budding profiles. Limiting MVB membrane (yellow), ILVs (red), vacuole (brown), nuclear envelope (blue), and class E compartments (green) are shown. Bars, 150 nm. (E) EM of cryofixed *vma4Δ* mutants or in combination with the indicated mutants. A, putative autophagosomal structures. Bars, 500 nm. (F) Mean diameters of ILVs inside the vacuoles of the respective *vma4Δ* mutants ($n = 50$). Error bars indicate the SDs. **, $P < 0.01$; ***, $P < 0.001$.

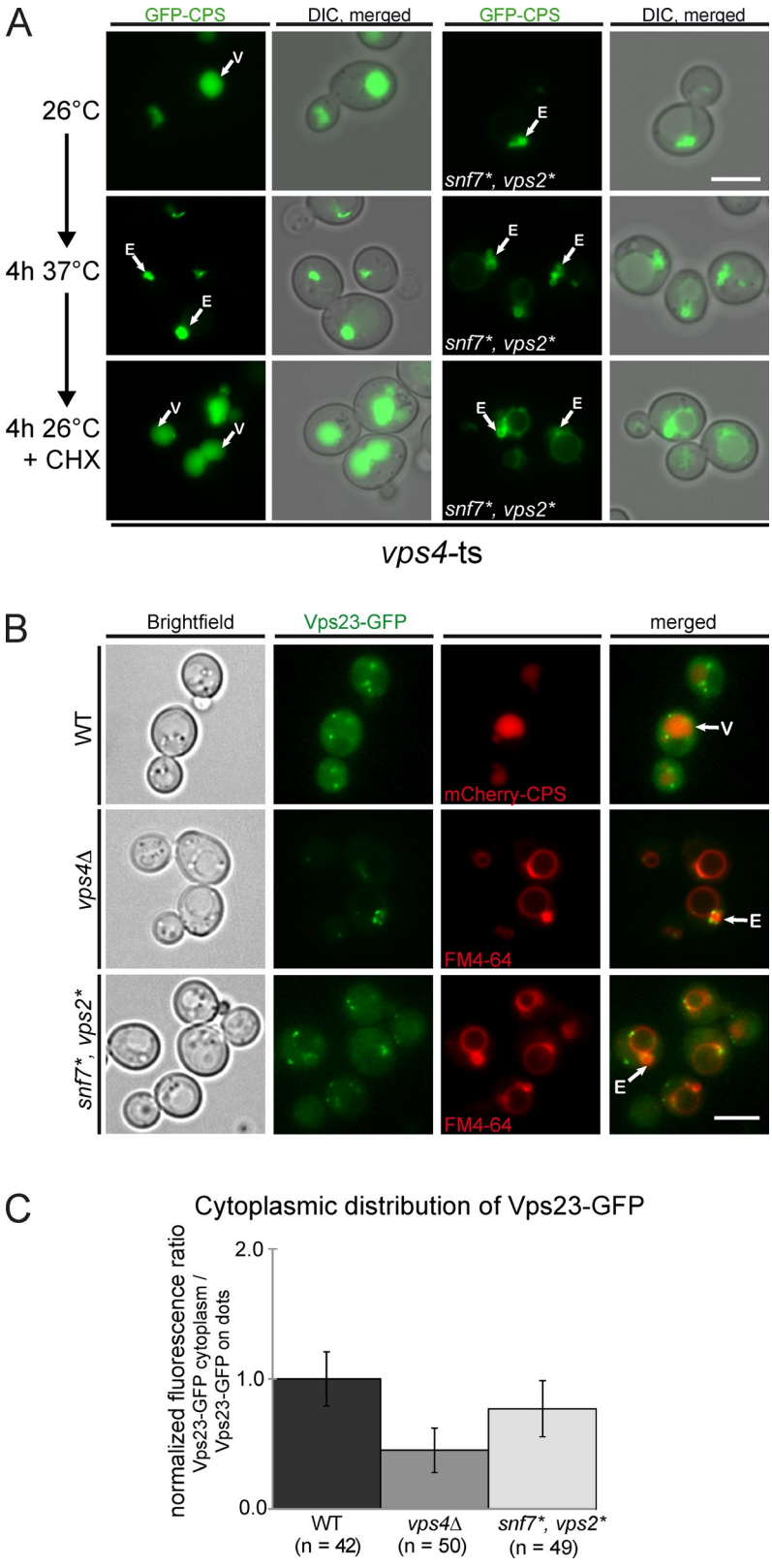


Figure S5. **Analysis of *snf7*, vps2** double mutants.** (A) *vps4*-ts mutants and *snf7*, vps2*, vps4*-ts mutants were grown at the permissive temperature and shifted to the nonpermissive temperature (37°C) for 4 h. 15 min before cells were shifted back to 26°C, 50 µg/ml cycloheximide (CHX) was added, and live-cell imaging of GFP-CPS of the corresponding strains at the indicated time points and growth conditions was performed. V, vacuole; E, class E; DIC, differential interference contrast. (B, top) Chromosomally integrated Vps23-GFP is functional and does not affect the transport of mCherry-CPS1 into the vacuole. In WT cells, the majority of Vps23-GFP was detected in the cytoplasm and sometimes on dots (endosomes). In *vps4Δ* mutants, Vps23-GFP accumulated on dots that colocalized with class E compartments. Little Vps23-GFP was in the cytoplasm. In *snf7*, vps2** mutants, Vps23-GFP was found not only on class E compartments but also in the cytoplasm. (C) Quantification of Vps23-GFP subcellular distribution. Fluorescence intensities of Vps23-GFP in ≥42 cells were measured in the cytoplasm and on dots. The ratio of the cytoplasmic signal/dots was normalized. SDs are shown. Bars, 5 µM.

Table S1. **SILAC-based quantification of Vps4-HA immunoprecipitation analysis using MaxQuant**

| Protein IDs | Protein descriptions | Ratio H/L normalized | Ratio H/L variability | Ratio H/L count | Peptide counts (all) | Sequence coverage | MM | Sequence length | PEP | Intensity | Intensity L | Intensity H |
|---|---|---|---|---|---|---|---|---|---|---|---|---|
| | | | % | | | % | *kD* | *aa* | | | | |
| **Vps4-HA IP WT (heavy) mixed with *vps2** (light)** | | | | | | | | | | | | |
| YPR173C | VPS4 | 1.1476 | 15.99 | 86 | 33 | 75.1 | 48.172 | 437 | $1.16 \times 10^{-221}$ | 7,035,200,000 | 3,608,100,000 | 3,427,000,000 |
| YMR077C | VPS20 | n. def. | n. def. | 0 | 1 | 4.5 | 25.638 | 221 | 0.088573 | 1,433,100 | 0 | 1,433,100 |
| YLR025W | SNF7 | n. def. | n. def. | 0 | 4 | 19.2 | 26.987 | 240 | $5.83 \times 10^{-21}$ | 6,366,300 | 0 | 6,366,300 |
| YKL041W | VPS24 | 14.907 | 11.966 | 11 | 11 | 50.4 | 26.242 | 224 | $3.56 \times 10^{-78}$ | 251,670,000 | 34,144,000 | 217,520,000 |
| YKL002W | DID4 | 29.205 | 10.419 | 8 | 11 | 31 | 26.29 | 232 | $2.08 \times 10^{-25}$ | 59,533,000 | 9,399,500 | 50133000 |
| YKR035W-A | DID2 | 10.385 | 21.009 | 10 | 10 | 42.2 | 23.091 | 204 | $1.05 \times 10^{-51}$ | 50,926,000 | 12,415,000 | 38511000 |
| **Vps4-HA IP WT (heavy) mixed with mock IP (no Vps4-HA; light)** | | | | | | | | | | | | |
| YPR173C | VPS4 | 69.612 | 164.56 | 27 | 38 | 80.5 | 48.172 | 437 | 0 | 4,098,400,000 | 260,570,000 | 1,205,500 |
| YMR077C | VPS20 | n. def. | n. def. | 0 | 1 | 12.2 | 25.638 | 221 | 0.20212 | 1,205,500 | 0 | 14,346,000 |
| YLR025W | SNF7 | n. def. | n. def. | 0 | 6 | 22.5 | 26.987 | 240 | $4.65 \times 10^{-42}$ | 14,346,000 | 0 | 60,564,000 |
| YKL041W | VPS24 | 4.6355 | 28.963 | 3 | 10 | 46.9 | 26.242 | 224 | $6.29 \times 10^{-67}$ | 63,883,000 | 3,318,800 | 21,128,000 |
| YKL002W | DID4 | n. def. | n. def. | 1 | 10 | 38.8 | 26.29 | 232 | $3.41 \times 10^{-33}$ | 21,510,000 | 381,720 | 16,752,000 |
| YKR035W-A | DID2 | n. def. | n. def. | 1 | 8 | 40.2 | 23.091 | 204 | $1.04 \times 10^{-57}$ | 20,506,000 | 3,754,400 | |

Relates to Fig. 1 D. H, heavy; IP, immunoprecipitation; L, light; MM, molecular mass; n. def., not defined; PEP, posterior error probability.

Table S2. **SILAC-based quantification of Vps4-HA immunoprecipitation analysis using Proteome Discoverer**

| Accession | Description | H/L | H/L variability | H/L count | No. of peptides | Coverage | MM | Sequence length | Score | Area (counts) |
|---|---|---|---|---|---|---|---|---|---|---|
| | | | % | | | | *kD* | *aa* | | |
| **Vps4-HA IP WT (heavy) mixed with *vps2** (light)** | | | | | | | | | | |
| YPR173C | VPS4 | 1.216 | 7.0 | 49 | 28 | 73.68 | 48.1 | 437 | 19,047.41 | $1.225 \times 10^{10}$ |
| YMR077C | VPS20 | n. def. | n.a. | 0 | 1 | 4.52 | 25.6 | 221 | 44.29 | $9.921 \times 10^{6}$ |
| YLR025W | SNF7 | n. def. | n.a. | 0 | 3 | 15.00 | 27.0 | 240 | 192.91 | $1.889 \times 10^{7}$ |
| YKL041W | VPS24 | 11.576 | 19.4 | 5 | 8 | 40.63 | 26.2 | 224 | 865.96 | $3.051 \times 10^{8}$ |
| YKL002W | DID4 | 18.499 | 0.3 | 2 | 9 | 26.72 | 26.3 | 232 | 583.16 | $3.462 \times 10^{8}$ |
| YKR035W-A | DID2 | 8.400 | 6.9 | 6 | 10 | 42.16 | 23.1 | 204 | 917.22 | $1.859 \times 10^{8}$ |
| **Vps4-HA IP WT (heavy) mixed with mock IP (no Vps4-HA; light)** | | | | | | | | | | |
| YPR173C | VPS4 | n. def. | n. def. | 0 | 34 | 76.89 | 48.1 | 437 | 17,618.14 | $1.081 \times 10^{10}$ |
| YLR025W | SNF7 | n. def. | n. def. | 0 | 5 | 18.33 | 27.0 | 240 | 329.52 | $2.181 \times 10^{7}$ |
| YKL041W | VPS24 | n. def. | n. def. | 0 | 6 | 33.93 | 26.2 | 224 | 550.72 | $1.158 \times 10^{8}$ |
| YKL002W | DID4 | n. def. | n. def. | 0 | 10 | 38.79 | 26.3 | 232 | 590.37 | $4.217 \times 10^{8}$ |
| YKR035W-A | DID2 | n. def. | n. def. | 0 | 8 | 40.20 | 23.1 | 204 | 466.84 | $7.211 \times 10^{7}$ |

Relates to Fig. 1 D. Accession numbers were obtained from the *Saccharomyces* Genome Database. H, heavy; IP, immunoprecipitation; L, light; MM, molecular mass; n.a., not annotated; n. def., not defined.

Table S3. **Yeast strains used in this study**

| Strain | Name | Genotype | Source |
|---|---|---|---|
| SEY6210.1 | WT | Mat a *leu2-3,112 ura4-52 his3-Δ200 trp1-Δ901 lys2-801 suc2-Δ9* | Robinson et al., 1988 |
| MBY3 | *vps4Δ* | SEY6210, *VPS4::TRP1* | Babst et al., 2002a |
| MBY4 | *vps4Δ* | SEY6210.1, *VPS4::TRP1* | Babst et al., 2002a |
| DTY65 | *vps2Δ* | SEY6210, *VPS2::HIS3* | Babst et al., 2002a |
| BWY101 | *vps25Δ* | SEY6210, *VPS25::HIS* | Babst et al., 2002b |
| MBY24 | *snf7Δ* | SEY6210.1, *SNF7::HIS3* | Babst et al., 2002a |
| DTY90 | *vps4Δ, snf7Δ* | MBY3, MBY24 | This study |
| MAY24 | *vps4Δ, vps20*$^{MIM1}$ | MBY3, *vps20-MIM1::TRP1* | This study |
| MAY28 | *vps2** | SEY6210.1, *vps2(L228D, K229D)::TRP1* | This study |
| MAY29 | *snf7** | SEY6210.1, *snf7(L199D)::TRP1* | This study |
| MAY27 | *vps24** | SEY6210.1, *vps24(R224D,L225D,L228D)::TRP1* | This study |
| MAY25 | *vps20** | SEY6210.1, *vps20(L188D)::TRP1* | This study |
| MAY91 | *snf7Δ, vps2** | MBY24, *vps2(L228D, K229D)::TRP1* | This study |
| MAY88 | *vps4Δ, snf7Δ vps2** | MAY91, MBY3 | This study |
| MAY58 | *vps4Δ, vps20** | MB3, MAY25 | This study |
| MAY40 | *vps4Δ, snf7** | MBY3, MAY29 | This study |
| MAY56 | *vps4Δ, vps24** | MBY3, MAY27 | This study |
| MAY39 | *vps4Δ, vps2** | MBY3, MAY28 | This study |
| MAY55 | *snf7*, vps2** | MAY39, MAY29 | This study |
| MAY72 | *vps4Δ, vps2*, snf7** | MAY39, MAY28 | This study |
| MAY67 | *vps24*, vps2** | MAY39, MAY27 | This study |
| MAY65 | *vps4Δ, vps20*, vps2** | MAY39, MAY25 | This study |
| MAY66 | *vps20*, vps24** | MAY58, MAY27 | This study |
| MAY68 | *vps4Δ, vps20*, vps24*, vps2** | MAY65, MAY66 | This study |
| MAY70 | *vps4Δ, vps20*, snf7*, vps24*, vps2** | MAY68, MAY29 | This study |
| MAY60 | *vps20*, snf7*, vps24*, vps2** | MAY68, MAY29 | This study |
| MAY52 | *vps20*, snf7*, vps24** | MAY68, MAY29 | This study |
| MAY69 | *vps4Δ, vps20*, snf7** | MAY68, MAY29 | This study |
| MAY51 | *vps4Δ, vps20*, snf7*, vps24** | MAY68, MAY29 | This study |
| MAY43 | *vps4Δ, vps20*, snf7*, vps2** | MAY68, MAY29 | This study |
| MAY53 | *snf7*, vps24*, vps2** | MAY68, MAY29 | This study |
| MAY54 | *vps4Δ, snf7*, vps24*, vps2** | MAY68, MAY29 | This study |
| MAY37 | *vps24*(ΔMIM)-Flag | SEY6210.1, *vps24-D209-FLAG::HIS3* | This study |
| DTY441 | *vma4Δ* | SEY 6210.1, *VMA4::URA3* | Teis et al., 2010 |
| DTY442 | *vma4Δ* | SEY 6210, *VMA4::URA3* | Teis et al., 2010 |
| DTY494 | *vma4Δ, vps20** | DTY442, MAY25 | This study |
| DTY491 | *vma4Δ, snf7** | DTY442, MAY29 | This study |
| DTY496 | *vma4Δ, vps20*, vps24** | DTY494, MAY27 | This study |
| MAY85 | *vps2*, vps20*$^{MIM1}$ | MAY28, *vps20-MIM1::TRP1* | This study |
| DTY492 | *vma4Δ, vps2** | DTY442, MAY28 | This study |
| DTY537 | *snf7Δ, vps2Δ* | MBY24, DTY65 | This study |
| MAY98 | *vps25Δ, vps2*, snf7** | MAY55, BWY101 | This study |

Table S4. **Plasmids used in this study**

| Plasmids | Description | Source |
|---|---|---|
| pMB31 | pGEX-KG, *GST-VPS4* | Babst et al., 1997 |
| ECE12 | pGEX-KG, *GST-vps4*$^{E233Q}$ | This study |
| pMA16 | pGEX-6P1, *GST-VPS2* | This study |
| pMA12 | pGEX-6P1, *GST-snf7*$^{MIM1}$ | This study |
| pMA13 | pGEX-6P1, *GST-snf7*$^{MIM1(L228D, K229D)}$ | This study |
| pDT56 | pGEX-KG, *GST-SNF7* | This study |
| pMA11 | pFA6a, *(VPS2)MIM1(L228D, K229D)::TRP1* | This study |
| pMA10 | pFA6a, *(VPS2)MIM1::TRP1* | This study |
| pMA43 | pFA6a, *snf7(L199D)::TRP1* | This study |
| pMA18 | pFA6a, *vps20(L188D)::TRP1* | This study |
| pMA19 | pFA6a, *vps24(R224D, L225D, L228D)::TRP1* | This study |
| pMA40 | pRS416, snf7$^{MIM1}$ | This study |
| pMA41 | pRS416, snf7$^{MIM1(L228D, K229D)}$ | This study |
| pOS063 | pRS415, *VPS4-HA* | This study |
| pMA25 | pGEX-KG, *GST-vps4*$^{L64D}$ | This study |
| pMA24 | pGEX-KG, *GST-vps4*$^{I18D}$ | This study |
| pMA48 | pRS416, *vps25*$^{T150K\text{-}Flag}$ | Teis et al., 2010 |
| pMA49 | prs415-$_{TDH3}$*GFP-VPS21* | This study |
| pMA50 | pRS414, *vps4*$^{E233Q}$ | This study |
| pMA51 | pGEX-6P1, *GST-vps2*-MIM2-MIM1 | This study |
| pMA52 | pGEX-KG, *GST-vps2*-MIM2 | This study |
| pMA53 | pRS415-$_{ADH1}$*vps2*-MIM2-MIM1 | This study |
| pMA54 | pRS415-$_{ADH1}$*vps2*-MIM2 | This study |
| pMA55 | pRS415-$_{ADH1}$*VPS2* | This study |
| pMA56 | pRS415-$_{ADH1}$*vps2*(1–214) | This study |
| pMA42 | pRS415, *vps4*$^{ts}$ | Babst et al., 1997 |
| pOS015 | pRS415, *vps4*$^{E233Q}$ | This study |
| pMP3 | pRS416, $_{TDH3}$*GFP-VPS21* | This study |
| pDT82 | pRS416, *VPS4-HA* | This study |
| pDT95 | pGEX-KG, *GST-VPS4-HA* | This study |
| pDT74 | pRS413, *VPS4-HA* | This study |
| pDT75 | pRS413, *vps4*$^{I18D}$*-HA* | This study |
| pDT76 | pRS413, *vps4*$^{L64D}$*-HA* | This study |
| pDT48 | pRS413, *vps4*$^{I18D, E233Q}$*-HA* | This study |
| pDT49 | pRS413, *vps4*$^{L64D, E233Q}$*-HA* | This study |
| pDT83 | pRS413, *vps4*$^{E233Q}$*-HA* | This study |
| pDN252 | *PGK1pr::RLuc SNA3-Fluc* (pDN251) | Nickerson et al., 2012 |
| pDT45 | pRS413, *vps4*$^{I18D}$ | This study |
| pDT46 | pRS413, *vps4*$^{L64D}$ | This study |

Table S5. **Primers used in this study**

| Primer name | Primer sequence (5′ → 3′) |
|---|---|
| VPS20-MIM2* forward | GATCTTAATTAAC**GAT**CCATCATTGCCTCAAGGAGAACAAA |
| Vps20-MIM2* reverse | GATCGGCGCGCCTCAGGATAGTAATGCTAAAGGTTCC |
| SNF7-MIM2* forward | GATCTTAATTAAC**GAT**CCTAGTGTTCCAAGTAATAAAATTA |
| SNF7-MIM2* reverse | GATCGGCGCGCCTCAAAGCCCCATTTCTGCTTGTAGT |
| Vps24-MIM1* forward | TAACAGGATGGTAAATGAAATGCGTGAA**GATGAC**AGAGCT**GAT**CAAAACTAGGG |
| Vps24-MIM1* reverse | CGCGCCCTAGTTTTG**ATC**AGCTCT**GTCATC**TTCACGCATTTCATTTACCATCCTTTAAT |
| Vps2-MIM1* forward | TAACGGTAATCCTGACGATGACTTGCAAGCTCGGTTGAACACT**GACGAT**AAGCAGACTTGAGG |
| Vps2-MIM1* reverse | CGCGCCTCAAGTCTGCTT**ATCGTC**AGTGTTCAACCGAGCTTGCAAGTCATCGTCAGGATTACCGTTAAT |
| Vps2-MIM1 forward | TAACGGTAATCCTGACGATGACTTGCAAGCTCGGTTGAACACTTTGAAGAAGCAGACTTGAGG |
| Vps2-MIM1 reverse | CGCGCCTCAAGTCTGCTTCTTCAAAGTGTTCAACCGAGCTTGCAAGTCATCGTCAGGATTACCGTTAAT |
| vps20GFPF2 | ACGGAGGAGAGATCAGACACTAAGGAACCTTTAGCATTACTATCCCGGATCCCCGGGTTAATTAA |
| vps20GFPR1 | GAAGGAACCTATTTACATTCCCTTTATTTTTAATTTTGAAGCTACGAATTCGAGCTCGTTTAAAC |
| Snf7_Sal1_forward | GAATGTCGACCAAGTTTTGACTTACAATTGCGGCT |
| Snf7-RIPGLIN-MIM1_reverse | TTAATTAACCCGGGGATCCGAAGCCCCATTTCTGCTTGTAGTTC |
| Snf7-RIPGLIN-MIM1_forward | GAACTACAAGCAGAAATGGGGCTTCGGATCCCCGGGTTAATTAA |
| *snf7*$^{MIM1}$_3_reverse | CTAAACCGCATAGAACACGTTCAAGTCTGCTTCTTCAAAG |
| Snf7_Spe1_reverse | GCCGACTAGTCGTTATTTGGGTTTTAGTCAATTAAAAGC |
| *snf7*$^{MIM1}$_3_forward | CTTTGAAGAAGCAGACTTGAACGTGTTCTATGCGGTTTAG |
| pGEX-6P1, Vps2 forward | GATCGGATCCATGAGTTTGTTTGAGTGGGTATTTG |
| pGEX-6P1, Vps2 reverse | GCTACTCGAGTCAAGTCTGCTTCTTCAAAGTGTTC |
| Vps2_Sal1_reverse | GATCGTCGACAACTTTAGTGACGAGATTGAG |
| Vps2ΔMIM1-reverse | CATTAAATATACTCAGAGCGCTCAATTACCGTGAAATTCTGATCCGGC |
| Vps2ΔMIM1-forward | GCCGGATCAGAATTTCACGGTAATTGAGCGCTCTGAGTATATTTAATG |
| Vps2_Xba1_forward | GATCTCTAGAATGAGTTTGTTGAGTGGGTATTTG |
| Vps2ΔMIM1-MIM2-MIM1 P1 | ATTACTTGGAACACTAGGTAGTGAGACTTTGTTCTCTGTTTCAGGAATCCCCATCGCTGT |
| Vps2ΔMIM1-MIM2-MIM1 P2 | TACCTAGTGTTCCAAGTAATAAAATTAAACAAAGTGAGCCTATTGGCGCCGGATCAGAAT |
| Vps2ΔMIM1-MIM2 P2 | TACCTAGTGTTCCAAGTAATAAAATTAAACAAAGTGAGTGAGCGCTCTGAGTATATTT |
| Vps2_BamH1_forward | GATCGGATCCATGAGTTTGTTTGAGTGGGTATTTG |
| Vps2-ΔMIM2-MIM2-MIM1_Xho1 reverse | CCCCGGGCTCGAGTCAAGTCTGTTTCTTCAAAGTGTT |
| Vps2-ΔMIM2-MIM2_Xho1 reverse | CCCCGGGCTCGAGTCACTCACTTTGTTTAATTTTATT |

Standard molecular biology was used to clone the ESCRT-III–MIM* tags into pFA6a-TRP1 Longtine vectors. The respective point-mutated codons are shown in bold (Leu199 in Snf7, Leu188 in Vps20, Arg224/Leu225/Leu228 in Vps24, and Leu228/Lys229 in Vps2). Vps20 was C-terminally MIM1 tagged by chromosomal integration. Standard molecular biology was used to clone *snf7*$^{MIM1}$/*snf7*$^{MIM1*}$ including the endogenous promoter and terminator into the pRS416 vector (the Vps2-MIM1 and -MIM1* fragments were amplified from the corresponding pFA6a-TRP1 Longtine cassettes): pRS416 5′-*snf7*-MIM1/*snf7*-MIM1*-3′. *snf7*-MIM1 and *snf7*-MIM1* were excised from the respective pRS416 plasmids and subcloned into pGEX-6P1. Standard molecular biology was used to clone *VPS2*/*vps2*(1–214) /*vps2*-MIM2 and *vps2*-MIM2-MIM1 under the control of an ADH1 promoter into the pRS415 vector. *vps2*-MIM2 and *vps2*-MIM2-MIM1 constructs were PCR amplified from the respective pRS415 plasmids and subcloned into pGEX-6P1.

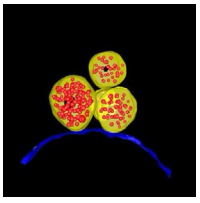

Video 1. **Electron tomography and 3D modeling of a cryofixed WT yeast cell overexpressing Vps21.** Set plane stepping followed by contour modeling of endosomal membranes (yellow), ILVs (red), and the nuclear envelope (blue) and stand-alone rotation of the contour model.

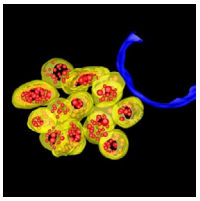

Video 2. **Electron tomography and 3D modeling of a cryofixed *snf7** mutant overexpressing Vps21.** Set plane stepping followed by contour modeling of endosomal membranes (yellow), ILVs (red), and the nuclear envelope (blue) and stand-alone rotation of the contour model.

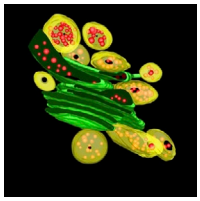

Video 3. **Electron tomography and 3D modeling of a cryofixed *vps2** mutant overexpressing Vps21.** Set plane stepping followed by contour modeling of endosomal membranes (yellow), ILVs (red), and the class E–like structure (green) and stand-alone rotation of the contour model.

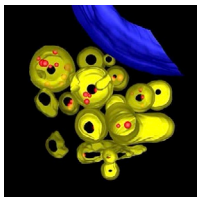

Video 4. **Electron tomography and 3D modeling of a cryofixed *snf7*, vps2** mutant overexpressing Vps21.** Set plane stepping followed by contour modeling of endosomal membranes (yellow), ILVs (red), and the nuclear envelope (blue) and stand-alone rotation of the contour model.

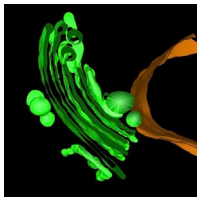

Video 5. **Electron tomography and 3D modeling of a cryofixed *snf7*, vps2*, vps25*$^{T150K}$ mutant overexpressing Vps21.** Set plane stepping followed by contour modeling of class E compartment (green) and the vacuolar membrane (brown) and stand-alone rotation of the contour model.

## References


Babst, M., T.K. Sato, L.M. Banta, and S.D. Emr. 1997. Endosomal transport function in yeast requires a novel AAA-type ATPase, Vps4p. *EMBO J.* 16:1820–1831. http://dx.doi.org/10.1093/emboj/16.8.1820

Babst, M., D.J. Katzmann, E.J. Estepa-Sabal, T. Meerloo, and S.D. Emr. 2002a. Escrt-III: an endosome-associated heterooligomeric protein complex required for mvb sorting. *Dev. Cell.* 3:271–282. http://dx.doi.org/10.1016/S1534-5807(02)00220-4

Babst, M., D.J. Katzmann, W.B. Snyder, B. Wendland, and S.D. Emr. 2002b. Endosome-associated complex, ESCRT-II, recruits transport machinery for protein sorting at the multivesicular body. *Dev. Cell.* 3:283–289. http://dx.doi.org/10.1016/S1534-5807(02)00219-8

Robinson, J.S., D.J. Klionsky, L.M. Banta, and S.D. Emr. 1988. Protein sorting in *Saccharomyces cerevisiae*: isolation of mutants defective in the delivery and processing of multiple vacuolar hydrolases. *Mol. Cell. Biol.* 8:4936–4948.

Teis, D., S. Saksena, B.L. Judson, and S.D. Emr. 2010. ESCRT-II coordinates the assembly of ESCRT-III filaments for cargo sorting and multivesicular body vesicle formation. *EMBO J.* 29:871–883. http://dx.doi.org/10.1038/emboj.2009.408